Agricultural Water Management 320 (2025) 109845

Contents lists available at ScienceDirect

Agricultural Water Management

journal homepage: www.elsevier.com/locate/agwat

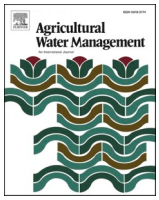

How reliable are long time-series reanalysis and model-based soil moisture products for agricultural soil water stress monitoring? Insights from a five-dataset evaluation across China

Peng Li [a,b], Liang He [c,*], Xuetong Wang [a,b], Ermao Ding [a], Qiang Yu [b,d,**]

[a] College of Natural Resources and Environment, Northwest A&F University, Yangling, Shaanxi 712100, China
[b] State Key Laboratory of Soil and Water Conservation and Desertification Control, Northwest A&F University, Yangling 712100, China
[c] National Meteorological Centre, Beijing 100081, China
[d] College of Resources and Environment, University of Chinese Academy of Sciences, Beijing 100049, China

ARTICLE INFO

Keywords:
Soil moisture trends
Long time-series monitoring
Agricultural water stress
Soil moisture product evaluation

ABSTRACT

Reliable soil moisture (SM) information underpins agricultural water management, yet large uncertainties remain in how long-term SM products capture hydroclimatic extremes. We systematically evaluate five widely used datasets—ERA5-Land (land reanalysis), GLEAM4 (satellite-driven water balance), GLDAS-Noah and GLDAS-CLSM (land surface models), and MERRA-2 (atmospheric reanalysis)—over China for 1982–2022. Using in situ observations, SMAP-L4 satellite data, and historical records of extreme droughts and floods, we assessed reliability against ground networks (Spearman ρ), consistency across products (Spearman ρ), and spatial coherence with SMAP-L4 (Pearson r). Long-term trends were quantified using the Theil–Sen estimator with the Trend-Free Pre-Whitening Mann–Kendall test. Results reveal a consistent divergence among products. MERRA-2, GLDAS-Noah, and GLEAM4 indicate widespread wetting, with positive SM trends across 33–75 % of grid cells and wet-stress intensification over 24–61 %. In contrast, ERA5-Land and GLDAS-CLSM depict drying, with negative SM trends over ~47–51 % of grids, drought intensification across 42–45 %, and declining wet stress in 30–40 %. ERA5-Land exhibits the strongest agreement with in situ data (median Spearman $\rho = 0.45$–0.48) and reliably captures benchmark extremes such as the 1998 Yangtze flood and the 2022 drought. MERRA-2 best matches SMAP-L4 (Pearson $r > 0.76$ nationwide) but underrepresents persistent droughts. Collectively, these findings establish ERA5-Land as the most reliable long-term benchmark for trend analysis, while underscoring the comparative advantage of MERRA-2 for short-term anomaly detection. Significant discrepancies in transitional and irrigated zones (e.g., the Loess Plateau and Huang–Huai–Hai Plain) underscore the need for climate- and region-specific fusion strategies.

1. Introduction

Agricultural production systems are increasingly vulnerable to hydroclimatic extremes, especially in water-limited and irrigated regions. The intensification and increased frequency of extreme hydroclimatic events—such as droughts (Chen et al., 2025), floods (Guo et al., 2025), and heavy rainfall (Shu et al., 2025; Wang, 2025)—have been widely observed in recent years (Schroeter et al., 2025; Wang et al., 2022). These events have caused substantial agricultural disruption, economic loss, and infrastructure damage, thereby exacerbating the burden on adaptation and risk management systems (Edwards et al., 2019; Hu et al., 2016; Khan and Islam, 2025). In this context, soil moisture (SM) has emerged as a critical variable for monitoring both real-time hydrometeorological stress and long-term shifts in land surface water availability. Importantly, it also underpins the quantification of key hydroclimatic extremes—such as drought and wet stress severity—over time, making its temporal characterization essential for climate impact assessments and disaster risk management, and agricultural water use planning (Kaur et al., 2017; Řehoř et al., 2023; Zhang et al., 2022). Drought is commonly classified into four categories: meteorological, agricultural, hydrological, and socio-economic. Meteorological drought results from imbalances between precipitation and

* Corresponding author.
** Corresponding author at: State Key Laboratory of Soil and Water Conservation and Desertification Control, Northwest A&F University, Yangling 712100, China
E-mail addresses: heliang@cma.gov.cn (L. He), yuq@nwafu.edu.cn (Q. Yu).

https://doi.org/10.1016/j.agwat.2025.109845
Received 30 July 2025; Received in revised form 21 September 2025; Accepted 22 September 2025

evapotranspiration, while agricultural drought occurs when SM is insufficient to meet crop water requirements (Wang et al., 2025). In this study, soil water stress refers to anomalies in either direction relative to long-term baselines—deficit (drought stress) or excess (wet stress). Although their mechanisms differ, both can severely affect crop growth, alter irrigation requirements, and increase agricultural risk.

Reliable and consistent long time-series SM datasets are essential not only for detecting hydroclimatic trends and extremes, but also for informing agricultural drought management and irrigation decision-making. Four primary types of products are commonly used: (1) in-situ observations, (2) satellite-based retrievals, (3) land surface model outputs, and (4) data assimilation and reanalysis products. In-situ observations offer high point-level accuracy but are spatially sparse and temporally discontinuous, which limits their direct use in large-scale analyses (Hong et al., 2024). Nevertheless, they are frequently employed as ground-truth references for validating remote sensing and model-derived SM products (Albergel et al., 2012; Ling et al., 2021; Zeng et al., 2015). Satellite datasets, such as ESA CCI SM, offer broad spatial coverage but often suffer from retrieval gaps and temporal inconsistencies due to cloud contamination, surface heterogeneity, and the limited revisit cycles of passive microwave sensors (Dorigo et al., 2015, 2017). Meanwhile, model-based and assimilation datasets deliver improved spatial-temporal coherence, offering seamless daily coverage with high spatial and temporal resolution, which makes them particularly useful for evaluating the evolution of drought and wet stress severity.

Despite the availability of high-resolution SM datasets from diverse sources, substantial inter-product differences persist in the estimation of long-term trends and hydroclimatic variability. Numerous studies have evaluated the temporal dynamics of SM using satellite, reanalysis, assimilation, and land surface model–based products. Global-scale analyses have revealed widespread drying trends over the past four decades, particularly in North America, northeastern Asia, and North Africa, although substantial regional discrepancies remain depending on the dataset used (Guan et al., 2023; Liu et al., 2019). Multi-dataset comparisons have shown generally high correlations in some regions such as northeastern Asia and parts of Australia, but poor agreement in others, including China's irrigated zones, where anthropogenic factors such as irrigation significantly influence SM trends (Luo et al., 2021; Qiu et al., 2016). Satellite-derived products such as ESA CCI SM have demonstrated strengths in detecting spatial drought severity patterns, while reanalysis-based products and data assimilation systems like GLDAS or MERRA offer better temporal coherence in densely vegetated areas (Albergel et al., 2013; Liu et al., 2019). However, inter-product trend consistency remains limited, especially in transitional climate zones and semi-arid regions, where drying signals are strongest but most variable (Dorigo et al., 2012; Rahmani et al., 2016). Some studies also report that long time-series SM trends—and their sensitivity to climate drivers such as ENSO—vary markedly depending on the chosen dataset (Guan et al., 2023; Xu et al., 2025), underscoring the methodological challenges in using SM for climate impact attribution. Products such as ESA CCI COMBINED and ERA5-Land have been shown to exhibit widespread drying trends over nearly half of the global land surface, whereas MERRA-2 and ESA CCI ACTIVE tend to indicate more extensive wetting. These inconsistencies—partly driven by systematic biases in precipitation and temperature forcing—directly affect the magnitude and spatial pattern of drought detection, with ESA CCI COMBINED capturing stronger drought signals compared to other products (Hirschi et al., 2025). While prior studies have advanced our understanding of product-specific trends, limited attention has been paid to how these differences propagate into hydroclimatic extreme metrics. Notably, the long-term evolution of drought and wet stress intensity derived from SM products remains insufficiently explored across datasets, revealing a critical and understudied dimension of hydroclimatic variability. This uncertainty poses challenges for drought risk evaluation, particularly in agricultural zones where water decisions depend on SM-derived indicators.

To address these gaps, this study systematically evaluates the spatial coherence and trend reliability of long time-series SM products for detecting drought and wet stress patterns across China—a region characterized by complex climatic gradients and frequent hydroclimatic extremes. Five widely used, gap-free, high-resolution daily SM datasets are analyzed over the period 1982–2022, including ERA5-Land (reanalysis), GLEAM4 (satellite-driven water balance model), GLDAS_Noah and GLDAS_CLSM (land surface model outputs), and MERRA-2 (atmospheric reanalysis). This study conducts a comprehensive assessment focusing on three key aspects: (1) Comparing the spatial divergence and consistency of trends in SM, drought intensity, and wet stress severity across multiple products; (2) Quantifying product-specific trend uncertainties using in situ observations from manual and automated monitoring stations, supplemented by SMAP L4 satellite data; (3) Evaluating performance of each product in identifying extreme hydroclimatic events, using representative summer drought and flood year in the Yangtze River Basin. Notably, to ensure statistically robust trend estimation across datasets with varying temporal structures, the analysis employs a dual-scale approach: annual trends for long time-series but coarser-resolution datasets, and monthly trends for high-resolution datasets with shorter durations. The findings offer a benchmark for evaluating the reliability of SM products in agricultural drought monitoring and water stress assessments, supporting their use in agro-hydrological planning across China.

2. Materials and methods

2.1. Study area

China has been divided into nine major agro-ecological zones based on biogeographical, climatic, and agricultural production characteristics (Fig. 1) (Han et al., 2024). These zones include: the Northeast China Plain (A), the northern arid and semiarid region (B), the Huang-Huai-Hai Plain (C), the Loess Plateau (D), the Qinghai–Tibet Plateau (E), the middle–lower Yangtze Plain (F), the Sichuan Basin and surrounding regions (G), Southern China (H), and Yunnan-Guizhou Plateau (I). This delineation reflects major differences in cropping systems, irrigation intensity, and climate exposure. The zonation is adopted from the Resource and Environment Science and Data Center of the Chinese Academy of Sciences (https://www.resdc.cn).

2.2. Datasets

2.2.1. In-situ observation datasets

This study employed two types of in-situ SM datasets from the China Meteorological Administration (CMA): manual observations (1980–2010) and automated measurements (2010–2022) (Fig. 1). The manual dataset comprises SM records on the 8th, 18th, and 28th of each month at five standard depths (10–100 cm), using the gravimetric-thermometric method and serving as a national benchmark (Wang and Shi, 2019). To ensure statistical robustness, a total of 122 sites were selected, each with at least two observations per month and a minimum of 20 consecutive years of data, from which annual mean SM was derived. Additionally, the automated dataset includes daily 0–10 cm SM from 480 stations (Li et al., 2022). Sites with at least two-thirds valid daily records per month and at least three consecutive years were retained, and monthly averages were computed. For both datasets, only surface (0–10 cm) SM was used in the product evaluation. Manual gravimetric-thermometric measurements are generally considered highly accurate and serve as the national benchmark dataset, but they are limited by low temporal frequency and potential observer-dependent biases. By contrast, automated stations provide higher-frequency daily measurements and much denser spatial coverage, yet the sensors are more susceptible to calibration drift and environmental noise, leading to larger uncertainties in long-term

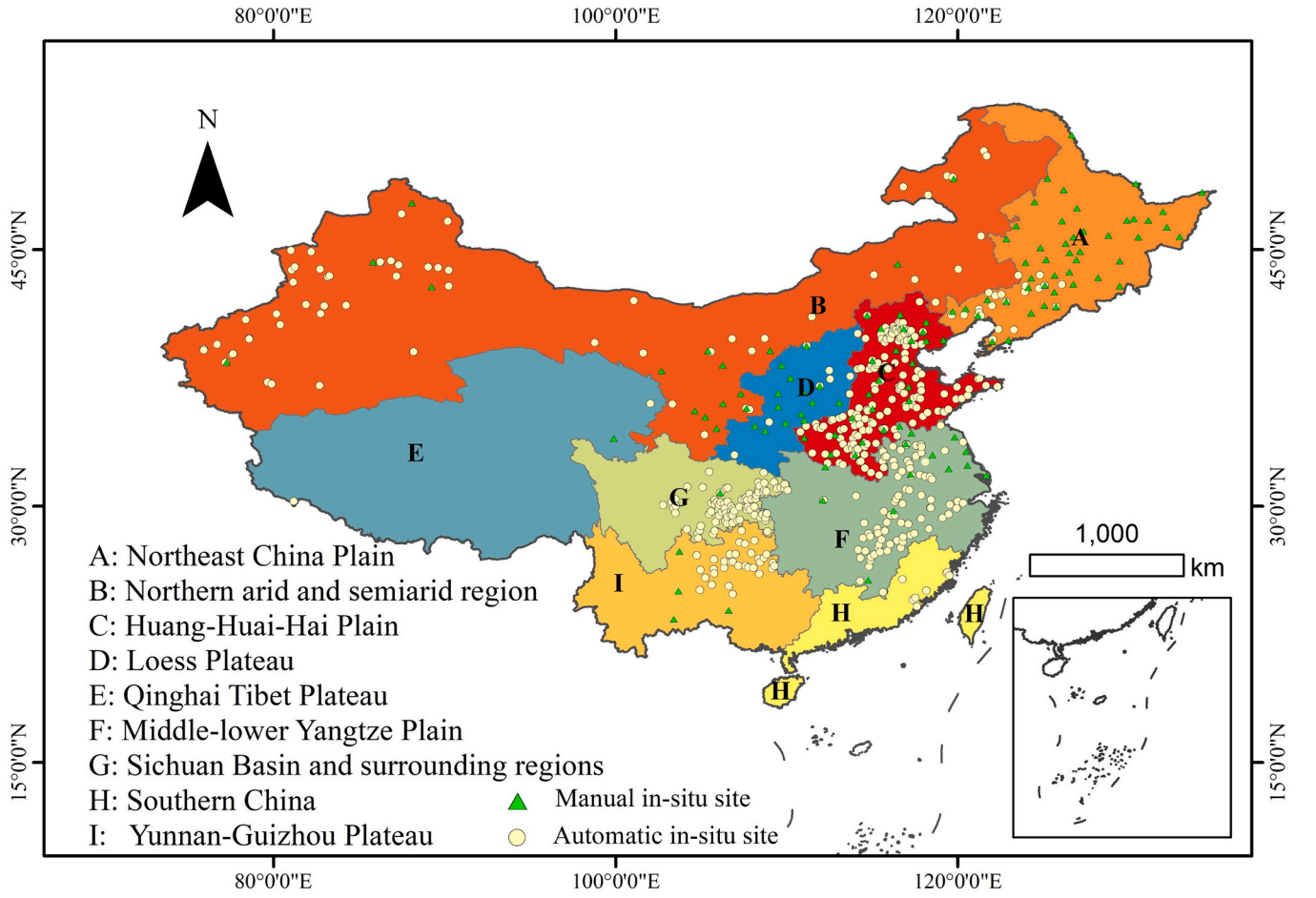

Fig. 1. Study area and regional division scheme used in this study. The nine agro-ecological zones (A–I) represent distinct climate and geographical regions of China, including the Northeast China Plain (A), Northern arid and semiarid region (B), Huang-Huai-Hai Plain (C), Loess Plateau (D), Qinghai-Tibet Plateau (E), Middle-lower Yangtze Plain (F), Sichuan Basin and surrounding regions (G), Southern China (H), and Yunnan-Guizhou Plateau (I).

consistency. These characteristics highlight a trade-off between accuracy and temporal/spatial coverage in the two observation systems.

2.2.2. *Five long time-series SM products*

This study uses five widely adopted, long time-series, daily SM products: ERA5-Land, GLEAM4, GLDAS_Noah, GLDAS_CLSM, and MERRA-2 (Table 1). To ensure temporal consistency, all products were temporally aggregated to a daily resolution using the arithmetic mean. This study focused on the surface SM layer provided by each product, as this depth is the most consistently defined across datasets and is the most directly observed or assimilated, whereas deeper layers are generally derived through model parameterizations and depend on surface estimates. Moreover, the 0–10 cm layer responds most rapidly to precipitation and evapotranspiration anomalies, making it a sensitive indicator of soil water stress.

ERA5-Land, developed by ECMWF, applies the HTESSEL land surface scheme with a four-layer soil structure and Darcy-based water flux formulation. It does not assimilate SM observations but is driven by high-resolution atmospheric inputs (Hersbach et al., 2020; Muñoz-Sabater et al., 2021).

GLEAM4 is a satellite-constrained diagnostic model that reconstructs SM based on passive microwave retrievals and partitioned evapotranspiration using the Priestley–Taylor method. It simulates key hydrological processes but omits state assimilation (Martens et al., 2017; Miralles et al., 2025).

GLDAS, developed by NASA, provides multiple land surface model outputs forced by observational data. This study utilizes two configurations: the Noah model, based on Richards equation with four soil layers and Penman–Monteith evapotranspiration (Zeng and Decker, 2009), and the CLSM, which uses a hydrologic response unit (HRU) approach with shallow top layers and explicit runoff-groundwater interaction (Jose et al., 2024). Neither GLDAS version incorporates

Table 1
Summary of the SM datasets used in this study.

Product	Type of product	Spatial resolution	Temporal resolution	**Surface soil depth**	Main reference
ERA5-Land	Land-surface reanalysis	0.1°	Hourly	0–7 cm	(Muñoz-Sabater et al., 2021)
GLEAM4	Hybrid satellite-based water balance mode	0.1°	Daily	0–10 cm	(Miralles et al., 2025)
GLDAS_ Noah	Land data assimilation model	0.25°	3-hourly	0–10 cm	(Rodell et al., 2004)
GLDAS_ CLSM	Catchment-based land surface model	0.25°	3-hourly	0–2 cm	(Rodell et al., 2004)
MERRA−2	Atmospheric reanalysis	0.5° × 0.625°	Hourly	0–5 cm	(Gelaro et al., 2017; Reichle et al., 2017)

direct SM assimilation.

MERRA-2, also from NASA, is an atmospheric reanalysis system built on the GEOS-5 framework. It uses the same Catchment LSM as GLDAS_CLSM but includes assimilation of microwave radiances and precipitation, targeting improved closure of land-atmosphere water budgets (Gelaro et al., 2017; Reichle et al., 2017).

2.2.3. SMAP L4 datasets

SMAP Level-4 (SMAP-L4) is a seamless, 3-hourly SM product at 9 km spatial resolution, operational since 31 March 2015. It integrates NASA's CLSM with assimilated satellite brightness temperature, improving SM estimates over the satellite-only Enhanced Level-3 product (Chan et al., 2018). Validation in China shows SMAP-L4 achieves lower bias and RMSE, and better captures daily precipitation dynamics than ERA5-Land, GLDAS_Noah, and GLEAM (Hong et al., 2024). In this study, monthly mean surface SM (0–5 cm) from March 2015 to December 2022 was extracted to assess product-level uncertainty.

2.3. Methods

2.3.1. Standardized Soil Moisture Index (SSMI)

To harmonize the scale of multi-source SM products and eliminate long-term trends, a three-step normalization and standardization procedure was applied at the grid-cell level over the full time series (Konkathi and Karthikeyan, 2024):

First, SM values were rescaled to [0,1] using min–max normalization:

$$SM_{\text{norm}} = \frac{SM_t - SM_{\min}}{SM_{\max} - SM_{\min}} \tag{1}$$

where SM_t is the SM at time t, and SM_{min}, SM_{max} are the minimum and maximum values over the entire time series.

Second, normalized values were fitted to a Beta distribution to derive the cumulative distribution function (CDF):

$$P_t = F_{Beta}\left(SM_{norm.t}\right) \tag{2}$$

where P_t is the cumulative probability. When Beta fitting failed, the empirical CDF (ECDF) was used.

Finally, P_t was transformed into the SSMI using the inverse standard normal CDF:

$$SSMI_t = \Phi^{-1}(P_t) \tag{3}$$

This transformation yields SSMI values with zero mean and unit variance, facilitating inter-product comparison and integration.

2.3.2. Drought/Wet stress severity

Based on the SSMI values, drought and wet stress indicators were defined using ±1 as thresholds for moderate severity (Carrão et al., 2016). Days with SSMI < -1 indicated dry stress events, while SSMI $> +1$ indicated wet stress events. The cumulative severity of these events was quantified on monthly or annual scales.

Drought severity was calculated as the cumulative excess of SSMI values above the dry threshold:

$$I_{dry} = \sum_{SSMI_t > 1} (SSMI_t - 1) \tag{4}$$

Wet stress severity was calculated as the cumulative deficit of SSMI values below the wet threshold:

$$I_{wet} = \sum_{SSMI_t < -1} (-1 - SSMI_t) \tag{5}$$

.

2.3.3. Trend analysis

To assess long-term trends in hydroclimatic variables, the non-parametric Theil–Sen estimator (Vannest et al., 2012; Wang and Yu, 2005) was applied to derive monotonic trends in annual SM, y stress intensity, and wet stress intensity at the pixel level.

The slope β is defined as the median of all pairwise slopes between time steps:

$$\beta = median\left(\frac{X_j - X_i}{j - i}\right), 1 < i < j \leq \text{n} \tag{6}$$

where X_i and X_j are the values of the variable at years i and j, respectively.

To evaluate the significance of these trends, we applied the Trend-Free Pre-Whitening Mann–Kendall (TFPW-MK) test (Gavrilov et al., 2018; Ji et al., 2025; Yue and Wang, 2002). The TFPW-MK method removes the influence of serial autocorrelation by first estimating and eliminating lag-1 dependence, then applying the Mann–Kendall test to the adjusted series. This procedure has been shown to improve the robustness of trend detection in hydroclimatic time series compared to the classical MK test. Trends were considered statistically significant at the 0.05 level. The analysis focused on identifying spatial clusters of significantly increasing or decreasing trends to detect regional hydroclimatic shifts. All computations were performed in Python (SciPy and pymannkendall libraries), which provide implementations of both the Theil–Sen slope estimator and the TFPW-MK test.

2.3.4. Consistency assessment

Temporal consistency across SM products was evaluated using the Spearman rank correlation coefficient (Schober et al., 2018; Sedgwick, 2014). This non-parametric, rank-based method is robust to outliers and suitable for assessing agreement in surface SM, drought intensity, and wet stress intensity at the pixel level across product pairs.

The Spearman coefficient (ρ) quantifies the monotonic relationship between two time series X and Y, based on their ranked values:

$$\rho = 1 - \frac{6\sum_{i=1}^{n} d_i^2}{n(n^2 - 1)} \tag{7}$$

where $d_i = R(X_i) - R(Y_i)$ the rank difference at time step i, and n is the number of time steps.

Positive ρ values indicate consistent temporal co-variation, with values approaching + 1 reflecting stronger agreement. Negative values ($\rho < 0$) suggest inverse relationships, indicating disagreement between products.

2.3.5. Product and trend uncertainty assessment

The study first evaluated the consistency of trend variations across different SM products using Spearman rank correlation. Two complementary approaches were employed: first, station-level comparisons were conducted using in situ observations, with manually recorded SM analyzed on an annual basis and automated measurements assessed monthly depending on data availability; second, product-specific trends were compared against those from the SMAP L4 dataset.

To account for opposing dry and wet signals in SM dynamics, the Net Dry–Wet Intensity (NDWI) was introduced to aid in the interpretation of hydroclimatic imbalances and to enhance comparability among different products. This study further examined the correlation between NDWI and either observed or SMAP L4 SM trends to assess the extent to which each product captures directional changes in hydroclimatic regimes, thereby enabling robust uncertainty evaluation.

The NDWI was introduced as a composite indicator:

$$NDWI = I_{dry} - I_{wet} \tag{8}$$

where I_{dry} and I_{wet} represent cumulative dry and wet stress intensities, respectively. A positive NDWI indicates dominance of drying conditions, while negative values reflect increasing wet stress.

2.3.6. Evaluation of major drought and extreme wet events

The capability of SM products in capturing extreme hydroclimatic events was assessed by analyzing changes in summer (June–August) dry and wet stress intensities across the Yangtze River Basin over the period 1982–2022. Years exhibiting extreme values in either drought or wet stress intensity were identified as representative drought or flood events. The performance of each product was then evaluated based on its ability to reproduce these historical extremes. According to observational records and documented disaster events, the summer of 1998 is recognized as the most severe flood event during the study period, followed by 2022. In contrast, 2022 also marked the most intense regional drought on record, with 2006 and 2011 identified as additional years characterized by significant drought impacts. These benchmark years were used as reference cases for evaluating the products' sensitivity and consistency in detecting extreme SM anomalies.

3. Results

3.1. Spatial and seasonal heterogeneity in trend patterns across multiple SM products

A consistent pattern of hydrological stress response emerges across SM products: increases in SM are generally associated with reduced drought intensity and enhanced wet stress, while decreases correspond to intensified drought and alleviated wet conditions. Nonetheless, notable inter-product differences remain in the spatial extent and distribution of these changes, reflecting uncertainties in spatial response patterns. (Figs. 2 and 3). MERRA-2, GLDAS_Noah, and GLEAM4 showed extensive increases in SM across most provinces, with 75 %, 33 %, and 46 % of pixels indicating a positive trend, respectively, and fewer than 20 % of pixels indicating a negative trend (1 %, 15 %, and 17 %). In contrast, ERA5-Land and GLDAS_CLSM were dominated by significant decreases, with 47 % and 51 % of pixels showing negative trends and only 9 % and 18 % showing increases, respectively—primarily across semi-humid and humid regions of eastern China. Trends in drought and wet stress severity followed similar spatial distributions. In MERRA-2, drought severity decreased over 51 % of the domain, while increases occurred in only 1 % of pixels; wet stress severity increased in 61 % of pixels. GLDAS_Noah and GLEAM4 showed comparable patterns, with balanced drought trends (increases in 22 % and 17 %, decreases in 27 % and 24 %, respectively) but a clear dominance of increasing wet stress (24 % and 41 % of pixels). These changes aligned closely with corresponding shifts in SM. ERA5-Land and CLSM exhibited opposite behavior. Both datasets showed widespread drought intensification (42 % and 45 %) and declining wet stress (40 % and 30 %), consistent with observed reductions in SM. Positive SM trends were largely confined to the Tibetan Plateau, while negative trends extended across central and eastern China.

Seasonal trends, summarized in Table 2, further emphasize inter-product divergence. ERA5-Land and GLDAS_CLSM exhibit consistently dry conditions across all seasons, reflected by significant declines in SM, increased drought severity, and reduced wet stress. In contrast, GLEAM4 and MERRA-2 show widespread wetting tendencies, with significant increases in both SM and wet stress throughout the year. However, only MERRA-2 also presents a clear and significant decline in drought severity across all seasons. GLEAM 4, by comparison, shows mixed or non-significant drought trends despite consistent wetting signals. Noah displays greater seasonal variability, with SM increasing significantly in spring and winter, drought severity intensifying in summer and autumn, and wet stress strengthening in summer and winter. This mixed seasonal behavior results in a less coherent trend pattern compared to the other products.

Overall, SM products exhibit a consistent relationship between SM trends and hydrological stress responses: increases in SM are generally associated with reduced drought severity and enhanced wet stress, while decreases correspond to intensified drought and reduced wet stress. However, substantial differences are observed across products in terms of the magnitude and spatial distribution of these changes. MERRA-2, GLDAS_Noah, and GLEAM4 predominantly show increasing SM and wet stress, whereas ERA5-Land and GLDAS_CLSM are characterized by decreasing SM and increasing drought severity. Seasonal trends further vary among products, with differences in both the direction and consistency of changes across seasons.

3.2. Inter-product consistency in trend patterns

Inter-product agreement in hydroclimatic trend detection varies substantially across variables, regions, and dataset combinations (Fig. 4). Among all pairs, ERA5-Land and GLDAS_CLSM exhibit the strongest overall agreement, particularly for SM and drought severity. In eight out of nine regions and at the national scale, their correlation coefficients exceed 0.73 for SM and 0.65 for drought severity, indicating a consistently high level of inter-product coherence. For wet stress severity, higher agreement is observed between GLDAS_Noah and GLDAS_CLSM ($r > 0.69$), and between Noah and MERRA-2 ($r > 0.60$) in several regions. However, these pairs show markedly lower agreement in the Qinghai-Tibet Plateau (E), where SM correlations are not statistically significant and drought severity correlations remain weak (GLDAS_Noah–MERRA-2 $r = 0.42$). In the same region, ERA5-Land and GLEAM4 yield the highest correlation for SM ($r = 0.78$), while GLDAS_Noah and GLDAS_CLSM achieve stronger consistency in drought severity ($r = 0.60$).

The degree of agreement also varies significantly by region. Southern China (H) demonstrates the most consistent cross-product performance, with correlation coefficients ranging from 0.53 to 0.86 across all indicators. The Northeast China Plain (A) follows, with values between 0.43 and 0.90. In contrast, the Sichuan Basin and surrounding regions (G) exhibit pronounced inconsistencies, including multiple product pairs with negative correlations, particularly for drought and wet stress severity. Nonetheless, a few combinations still show moderate agreement in this region. Overall, across SM, drought severity, and wet stress, regional differences emerge as a consistent driver of inter-product agreement.

3.3. Uncertainty in SM and hydroclimatic stress trends based on station observations

Fig. 5a–e show the spatial distribution of Spearman correlation coefficients between annual SM from five gridded products and observations from manual meteorological stations during 1982–2022. High correlations for ERA5-Land and MERR-2 are concentrated in North China, Northeast China, and the middle–lower Yangtze River Basin, with more spatially continuous coverage. GLEAM4 shows more balanced distribution patterns, with moderately dense stations across several regions. In contrast, GLDAS_Noah and GLDAS_CLSM have fewer significant stations and more fragmented spatial coverage, particularly for GLDAS_CLSM. Fig. 5f–g summarize product dominance based on the highest and statistically significant station-level correlations. MERRA-2 ranks first at 33.7 % of stations, followed by ERA5-Land at 29.7 %. GLEAM4 (13.9 %), GLDAS_Noah (12.9 %), and GLDAS_CLSM (9.9 %) dominate fewer stations, with scattered spatial distributions and no clear regional clustering. Fig. 5 h compares overall performance across products. ERA5-Land and MERRA-2 have the highest median correlations and the narrowest interquartile ranges.

Fig. 6a–e show the spatial distribution of Spearman correlation coefficients between monthly SM from five gridded products and automatic in situ station observations. ERA5-Land exhibits higher correlations, with spatially coherent clusters across GLDAS_North China, the Huang-Huai Plain, Jianghuai, and the Yangtze River Basin. GLEAM4 shows a more scattered pattern, with moderate correlations in parts of eastern China but generally lower values. GLDAS_Noah and GLDAS_CLSM display fragmented spatial distributions, with only a few

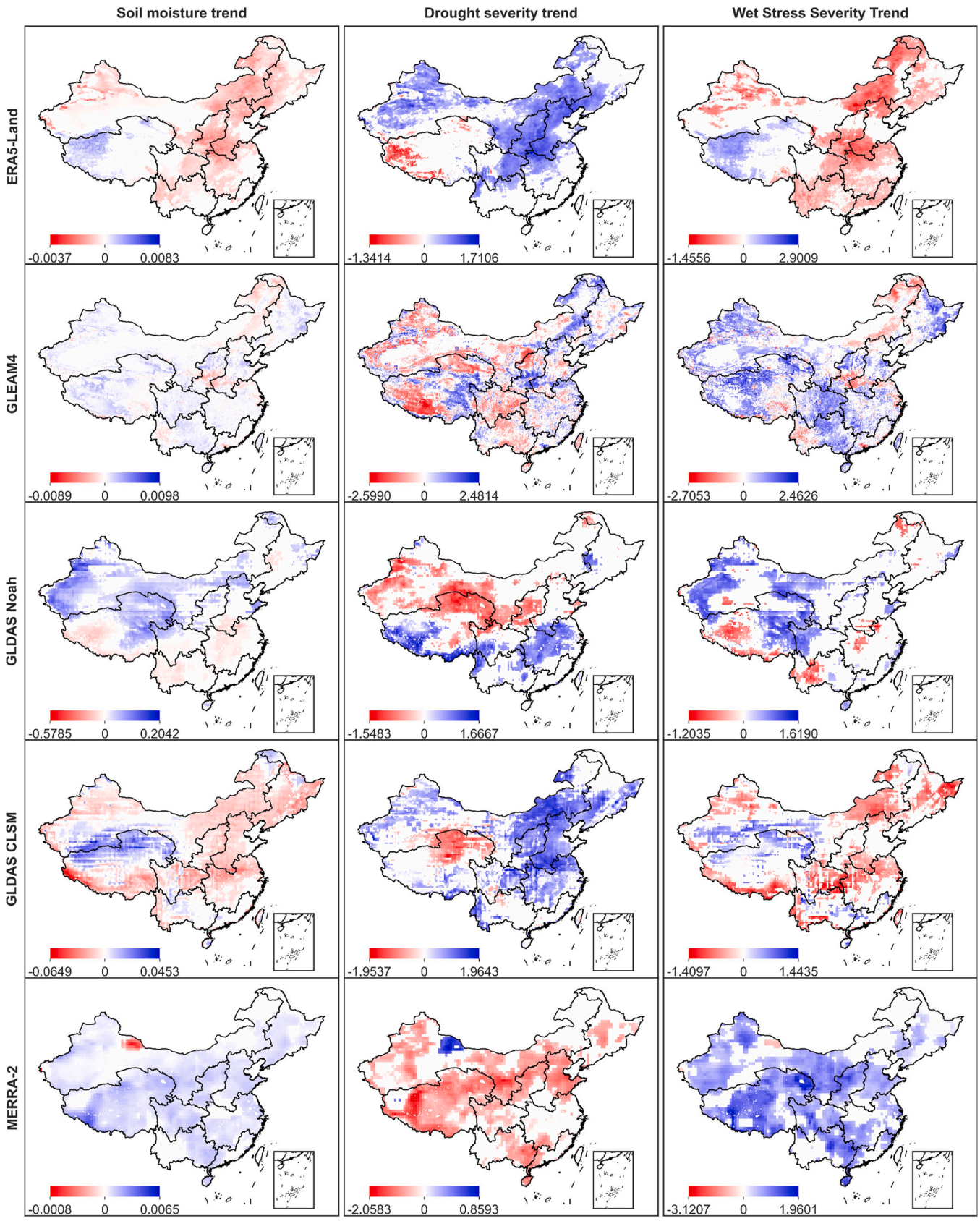

Fig. 2. Theil–Sen slope estimates with significance tested by the TFPW-MK method for annual mean SM, annual drought intensity, and annual wet stress intensity for each product. Zero values indicate pixels with no statistically significant trend ($p \geq 0.05$).

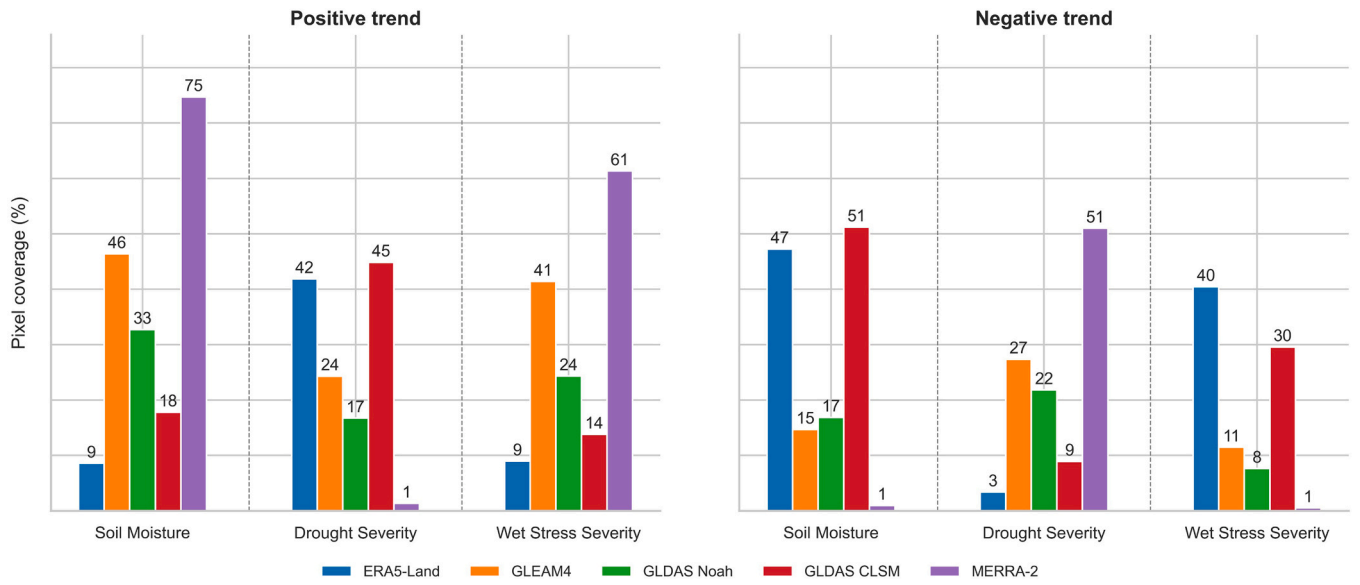

Fig. 3. Percentage of pixels exhibiting statistically significant positive and negative Theil–Sen trends (significance tested by TFPW-MK) in annual SM, drought intensity, and wet stress severity for each product during 1982–2022.

Table 2
Seasonal Theil–Sen slopes with significance tested by the TFPW-MK method for annual mean SM, drought intensity, and wet stress severity derived from five products across China. Seasons are defined as spring (March–May), summer (June–August), autumn (September–November), and winter (December–February, including December of the previous year).

	Trend / Season	ERA5-Land	GLEAM4	GLDAS _NOAH	GLDAS _CLSM	MERRA-2
SM	Spring	−0.0004***	0.0003***	0.0267**	−0.0048***	0.0006***
	Summer	−0.0002**	0.0003***	−0.003	−0.0044**	0.0007***
	Autumn	−0.0003*	0.0002**	0.0025	−0.0048**	0.0008***
	Winter	−0.0002	0.0002***	0.0188**	−0.0053***	0.0007***
Drought severity	Spring	910***	−288	−276	1712***	−1625***
	Summer	844***	−15	56**	1077***	−775***
	Autumn	505***	60	13*	246**	−334***
	Winter	73	−212	95	352***	−342***
Wet Stress Severity	Spring	−458**	506**	76	−517*	1376***
	Summer	−521***	213***	216*	−163**	216***
	Autumn	−721*	1251**	200	−462	2137***
	Winter	−118*	7**	36***	−19	112***

areas showing moderate correlations. MERRA-2 presents regional variability, with some stations showing positive correlations, but overall lacks spatial continuity or concentrated zones of higher agreement. Fig. 6f–g summarize the dominant product at each station based on the highest statistically significant correlation. ERA5-Land accounts for the largest share (48.4 %), primarily concentrated in North and East China. GLEAM4 (17.7 %), GLDAS_Noah (14.8 %), GLDAS_CLSM (10.7 %), and MERRA-2 (8.4 %) dominate fewer stations and show more scattered spatial distributions. Fig. 6 h presents boxplots comparing the overall distribution of correlation coefficients for each product. ERA5-Land shows the highest median and narrowest interquartile range, with few outliers, reflecting stable performance. GLEAM4 has the lowest median, indicating generally weaker correlations across stations.

Fig. 7 presents Spearman correlation density distributions between SM products and the NDWI. For manual stations (Fig. 7a), ERA5-Land shows the highest median correlation (0.45), with values concentrated between 0.4 and 0.6. GLDAS_Noah, GLDAS_CLSM, and MERRA-2 exhibit lower medians (0.38–0.39) and broader distributions. GLEAM4 has the lowest median (0.20) and the highest proportion of negative values (21 %). At automatic stations (Fig. 7b), all products display flatter, more dispersed curves. ERA5-Land retains the highest central tendency (median 0.45). GLDAS_Noah, GLDAS_CLSM, and MERRA-2 have similar ranges, while GLEAM4 remains the lowest and shows the most pronounced left skew.

Overall, results from both manual and automatic stations reveal clear inter-product differences in agreement with observations. ERA5-Land shows the highest consistency across scales, with strong correlations and low dispersion. MERRA-2 performs well annually but is less stable monthly. GLEAM4 yields weaker correlations and a higher share of negative values. GLDAS_Noah and GLDAS_CLSM display the most fragmented and variable agreement.

3.4. Uncertainty in SM and hydroclimatic stress trends based on SMAP L4 data

SMAP L4-based comparisons reveal clear inter-product differences in regional agreement across China (Fig. 8). For SM (Fig. 8a), MERRA-2 shows the strongest performance, with correlation coefficients exceeding 0.76 and full statistical significance in all regions. GLEAM4 ranks first only in Southern China (H, r = 0.80) but records the lowest average agreement overall. ERA5-Land shows moderate yet consistent correlations across all regions, all above 0.55 and statistically significant. GLDAS_CLSM and GLDAS_Noah yield comparatively lower values and no regional lead. For NDWI (Fig. 8b), MERRA-2 again ranks highest

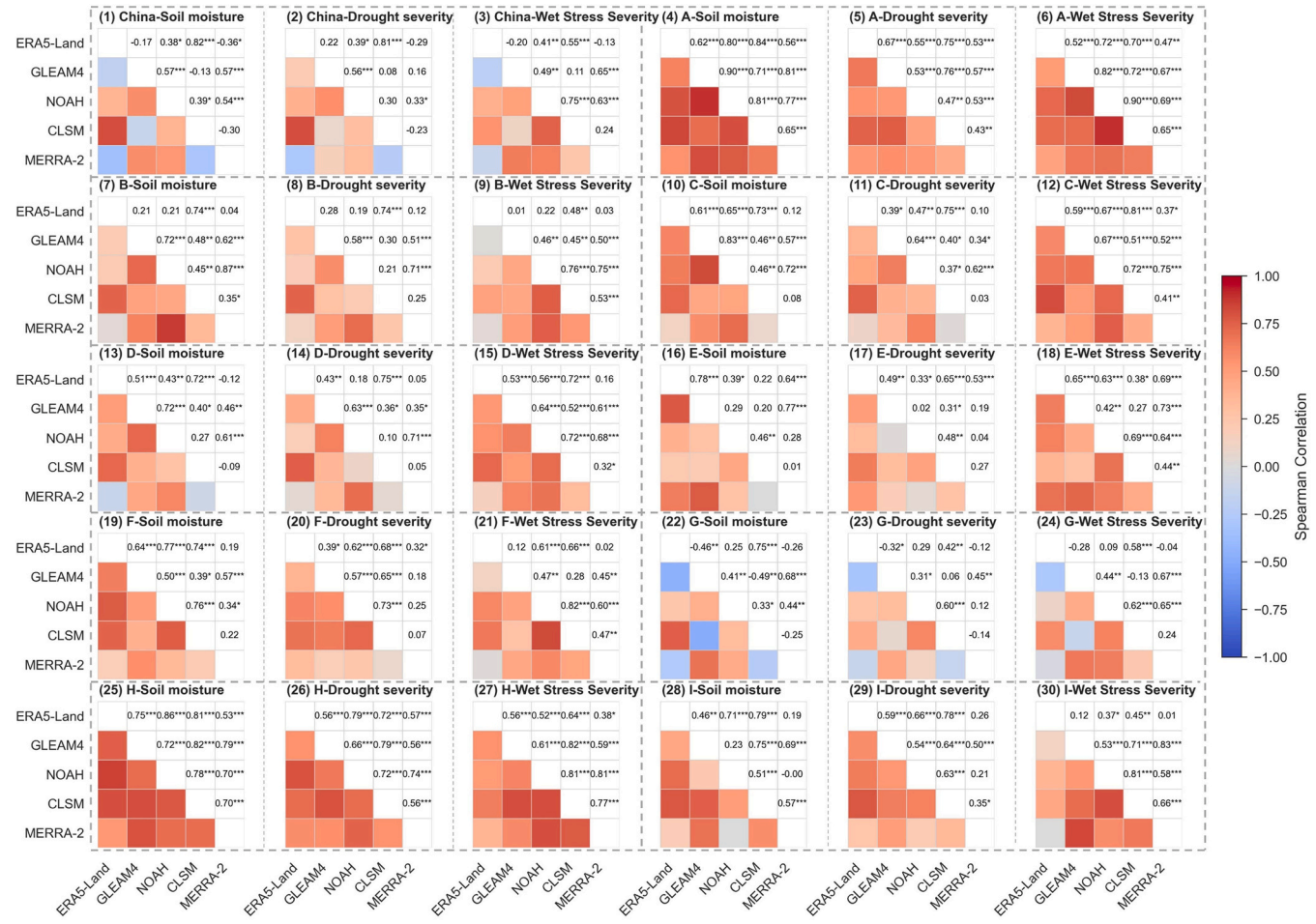

Fig. 4. Spearman correlation heatmaps between product pairs based on regional time series of annual mean SM, annual drought intensity, and annual wet stress severity across China from 1982 to 2022. Each panel shows pairwise correlation coefficients and corresponding significance levels for each variable. The sub-regions labeled A–I are defined as in Fig. 1.

in all nine regions, with correlations ranging from 0.70 to 0.96, all significant. GLDAS_CLSM follows with values between 0.60 and 0.88. ERA5-Land shows a lower national-scale correlation ($r = 0.41$) but exceeds 0.50 in every region. GLEAM4 drops to 0.20 in the Northern arid and semiarid region (B), though it remains above 0.55 elsewhere. GLDAS_Noah shows the weakest performance overall, with five regions below 0.50 and several non-significant correlations. These results identify MERRA-2 as the only product with consistent, high agreement with SMAP across both SM and dry–wet variability at the regional scale.

3.5. Evaluation of major drought and extreme wet events in the Yangtze River Basin

Fig. 9 presents the summer evolution of drought and wet stress severity over the Yangtze River Basin, focusing on five major hydroclimatic events. ERA5-Land identifies 2022 as the year of maximum drought severity and 1998 as the peak wet stress year. It also captures 2006, 2011, and 2020 with clearly separated intensity peaks. GLDAS_Noah detects drought intensification in 2006, 2011, and 2022, and marks 2022 as the driest year. It shows increased wet stress in 1998 and 2020, but does not distinguish 1998 as the most extreme. GLDAS_CLSM reflects elevated drought in 2022 and 2011 but not in 2006. It registers wet anomalies in 1998 and 2020, although other years exhibit higher wet stress values. GLEAM4 does not show distinct drought signals for 2006, 2011, or 2022, but registers 2020 as the year with maximum wet stress. The 1998 flood event is not clearly represented. MERRA-2 captures 2006 and 2011 drought peaks but does not identify 2022 as the most severe year. It reflects substantial wet stress in 1998 and 2020, though 1998 is not identified as the maximum. In summary, ERA5-Land reproduces all five target events with distinct responses in both drought and wet stress. GLDAS_Noah detects all drought years and partially responds to wet events. MERRA-2 and GLDAS_CLSM reflect subsets of events. GLEAM4 captures 2020 wet stress but does not resolve major drought signals.

4. Discussion

4.1. Divergence rooted in model design

The divergence among SM products across China arises not only from observational uncertainty or temporal aliasing, but more fundamentally from differences in how each model conceptualizes the soil–atmosphere system. Variations in model structure, soil layering, energy balance closure, and assimilation strategies drive distinct responses to climate forcing and hydrological memory representation. Grasping these design-level contrasts is key to interpreting long-term trend discrepancies and anomaly sensitivity across datasets ERA5-Land, developed by ECMWF, employs the HTESSEL model with a four-layer soil structure and simulates water fluxes via Darcy's law. Its topsoil layer (0–7 cm) dynamically interacts with high-resolution atmospheric forcing but does not directly assimilate SM (Hersbach et al., 2020; Muñoz-Sabater et al., 2021). This setup supports stable trend detection under persistent climate signals and aligns closely with manual in situ observations. ERA5-Land also reliably captures all benchmark hydroclimatic extremes examined in

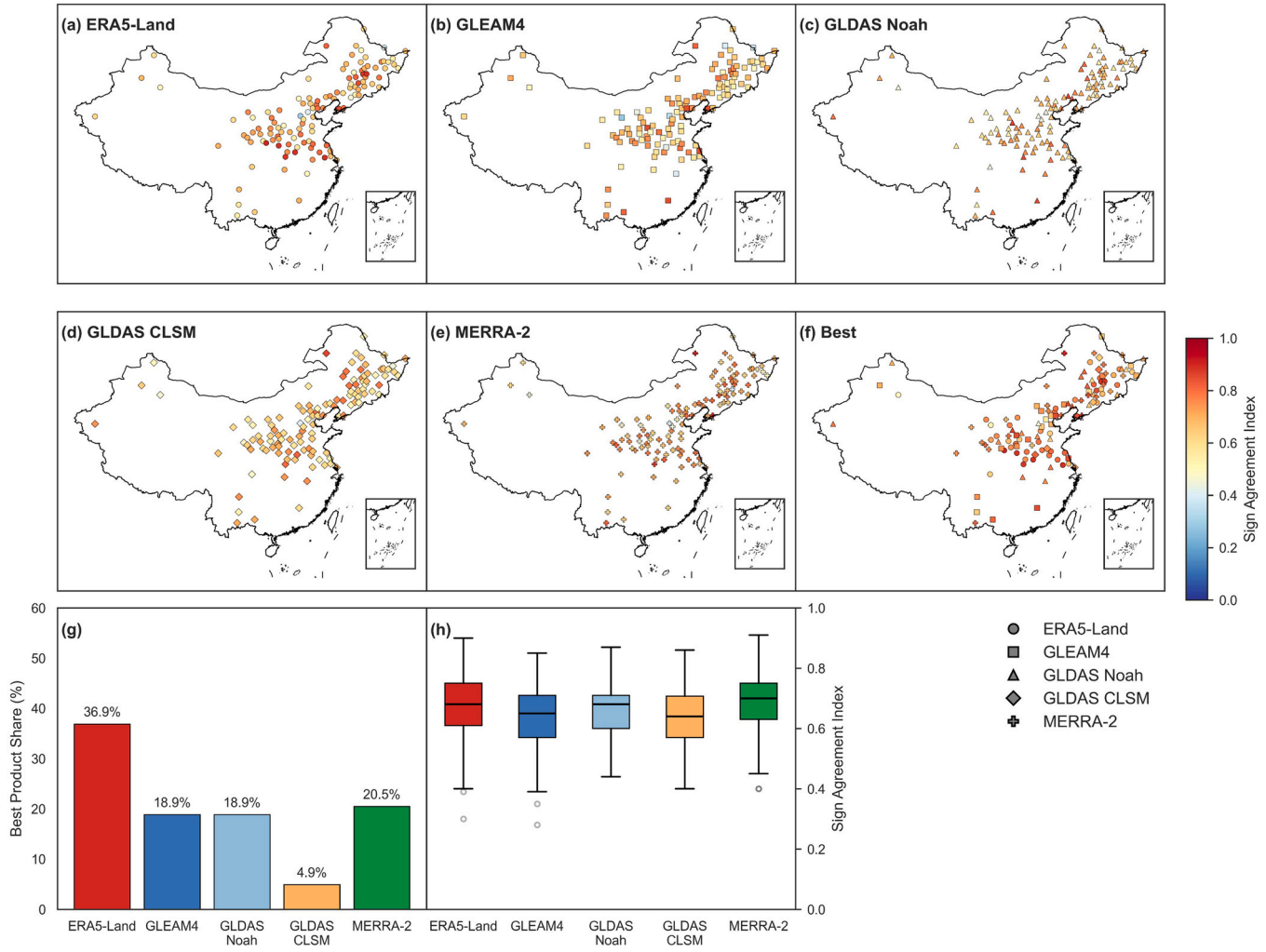

Fig. 5. (a–e) Spearman correlation coefficients between annual mean SM time series from in situ observations and individual products across all stations. (f) Spatial distribution of the product with the highest statistically significant correlation at each station. (g) Frequency distribution of the best-performing product across all stations. (h) Box plots showing the distribution of Spearman correlation coefficients between each product and the observed data.

this study, indicating strong temporal robustness. In contrast, NASA's MERRA-2 reanalysis, based on the GEOS-5 platform, uses the Catchment LSM, which realistically simulates shallow water tables and runoff. It directly assimilates microwave brightness temperatures and precipitation estimates (Gelaro et al., 2017), enhancing its sensitivity to transient anomalies—particularly convective precipitation—but also introducing high-frequency noise and trend instability, as seen in automatic station data. While MERRA-2 aligns well with SMAP for monthly anomalies, it underrepresents persistent extremes such as the 2022 drought and the 1998 flood.

GLEAM4, a satellite-constrained water balance model, reconstructs root-zone moisture using passive microwave inputs (e.g., SMOS, AMSR2) and Priestley–Taylor-based evaporation partitioning. It simulates canopy interception, snow sublimation, and runoff, but does not assimilate state variables (Martens et al., 2017; Miralles et al., 2025). This diagnostic framework captures vegetation-mediated SM dynamics in the 0–10 cm layer. Its strong response to the 2020 Yangtze flood reflects high flux sensitivity in wet regions, though it misses major droughts (2006, 2011, 2022) and shows the weakest correlation with in situ trends, especially in semi-arid zones. Under NASA's GLDAS framework, GLDAS_Noah and GLDAS_CLSM differ in model design. Noah features a four-layer structure governed by the Richards equation and Penman–Monteith evapotranspiration, while CLSM adopts a hydrologic response unit (HRU) scheme with shallow top layers (0–2 cm) and explicit modeling of saturated excess runoff (Jose et al., 2024; Rodell et al., 2004; Zeng and Decker, 2009). These structural differences shape trend expression. While GLDAS-CLSM mirrors ERA5-Land's long-term drying signal, it struggles with benchmark drought representation (e.g., 2006) and shows weaker agreement with station and NDWI trends.

While ERA5-Land provides high-resolution (0.1°) coverage and stable performance in long-term monitoring, uncertainties remain in regions with complex topography and sparse in situ constraints, such as the Qinghai–Tibet Plateau. In these areas, biases in precipitation forcing and limitations in representing frozen soil processes have been reported to reduce reliability (Hou et al., 2021; Niu et al., 2021) Similarly, GLDAS products offer the advantage of multi-model diversity and physically consistent hydrological schemes, but they do not assimilate soil moisture observations (Lucas et al., 2020; Rodell et al., 2004) and omit irrigation processes. This omission is particularly relevant for heavily irrigated zones such as the Huang-Huai-Hai Plain, where anthropogenic water use strongly modulates soil moisture dynamics, leading to systematic discrepancies relative to observations (Liu et al., 2025; Piao et al., 2010). These dataset-specific constraints need to be considered when applying SM products in agricultural water stress studies.

4.2. *Consistency, memory, and product behavior*

Although some SM products exhibit similar signs in long-term trends,

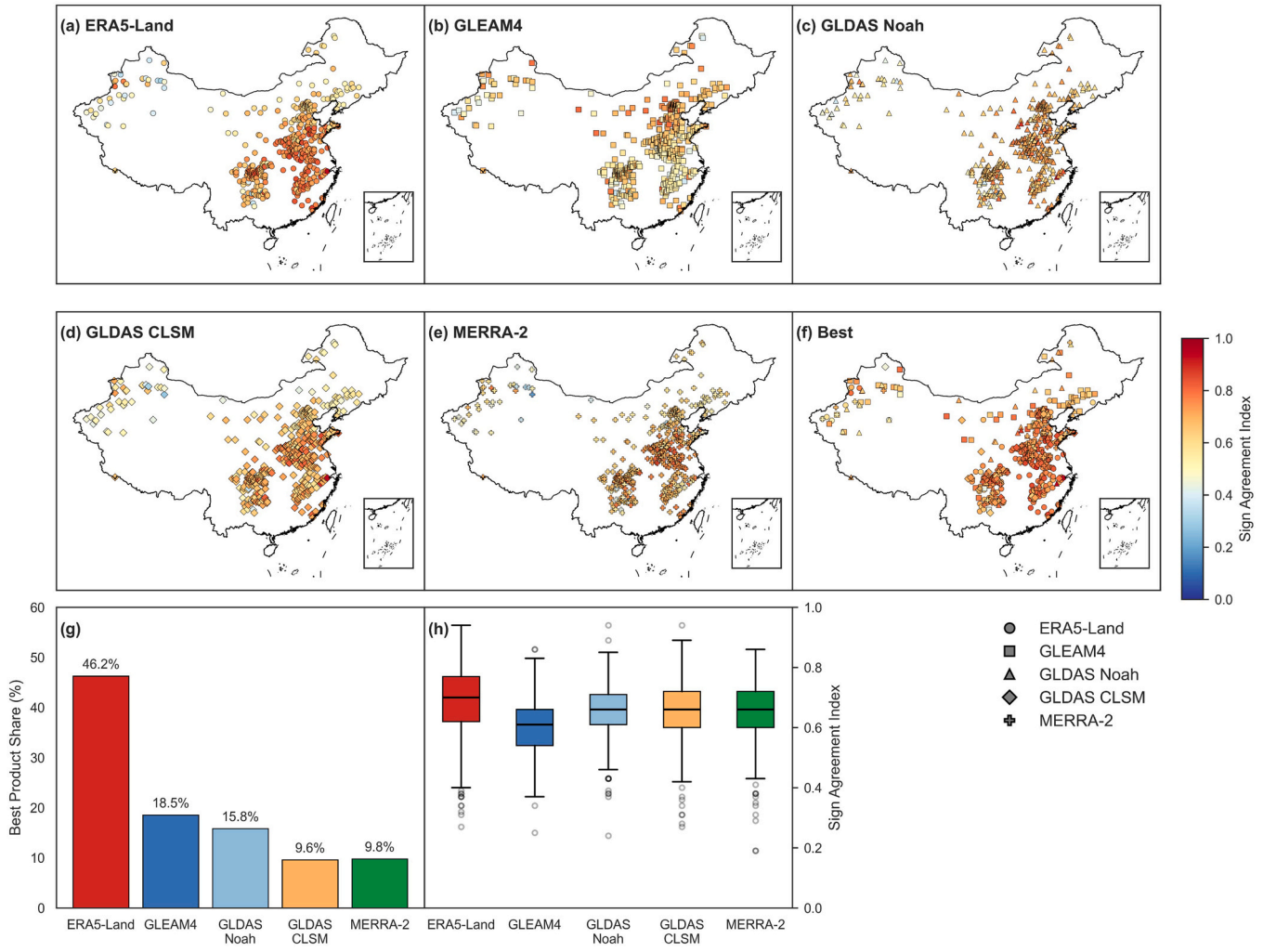

Fig. 6. (a–e) Spearman correlation coefficients between monthly mean SM time series from automatic in situ observations and individual products across all stations. (f) Spatial distribution of the product with the highest statistically significant correlation at each station. (g) Frequency distribution of the best-performing product across all stations. (h) Box plots showing the distribution of Spearman correlation coefficients between each product and the observed data.

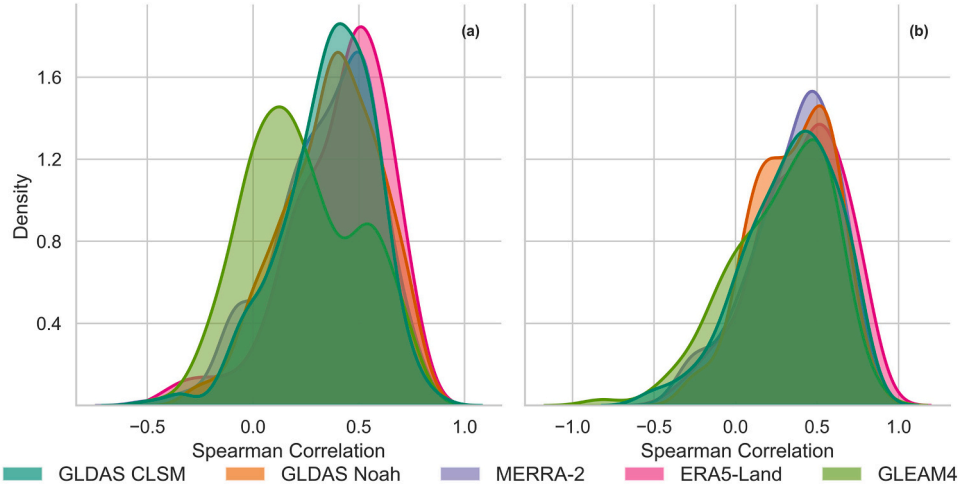

Fig. 7. Frequency distributions of Spearman correlation coefficients between observed SM and Net Dry–Wet Intensity (NDWI) time series, calculated at each station. These distributions are used to assess which product best captures the directional trend in hydroclimatic stress. (a) Correlations between annual mean SM and annual NDWI based on manually observed data. (b) Correlations between monthly mean SM and monthly NDWI based on automatically recorded data.

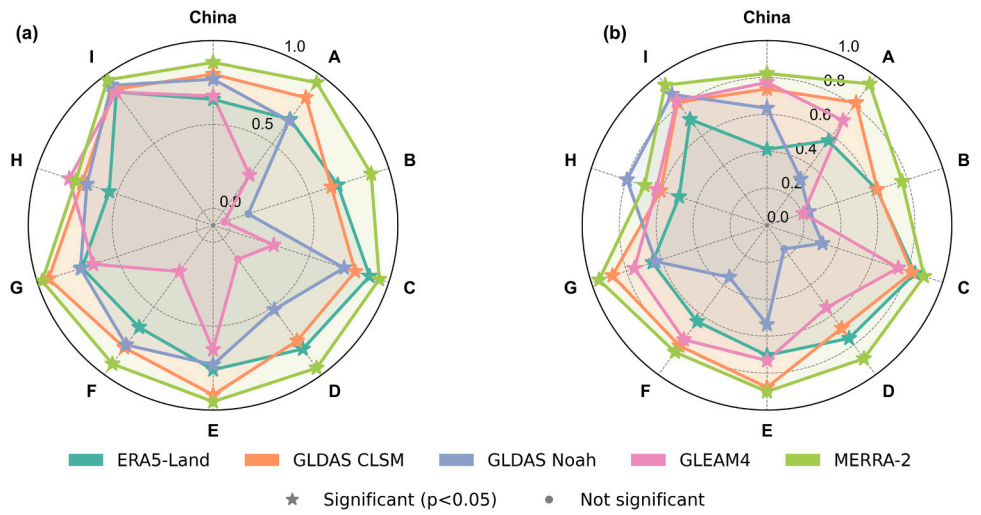

Fig. 8. Radar plots showing Spearman correlation coefficients between SMAP L4 data and other products based on monthly data from 2015 to 2022. (a) Correlations between monthly SM from SMAP and each product. (b) Correlations between SMAP monthly SM and the monthly Net Dry–Wet Intensity (NDWI) derived from each product. The sub-regions labeled A–I are defined as in Fig. 1.

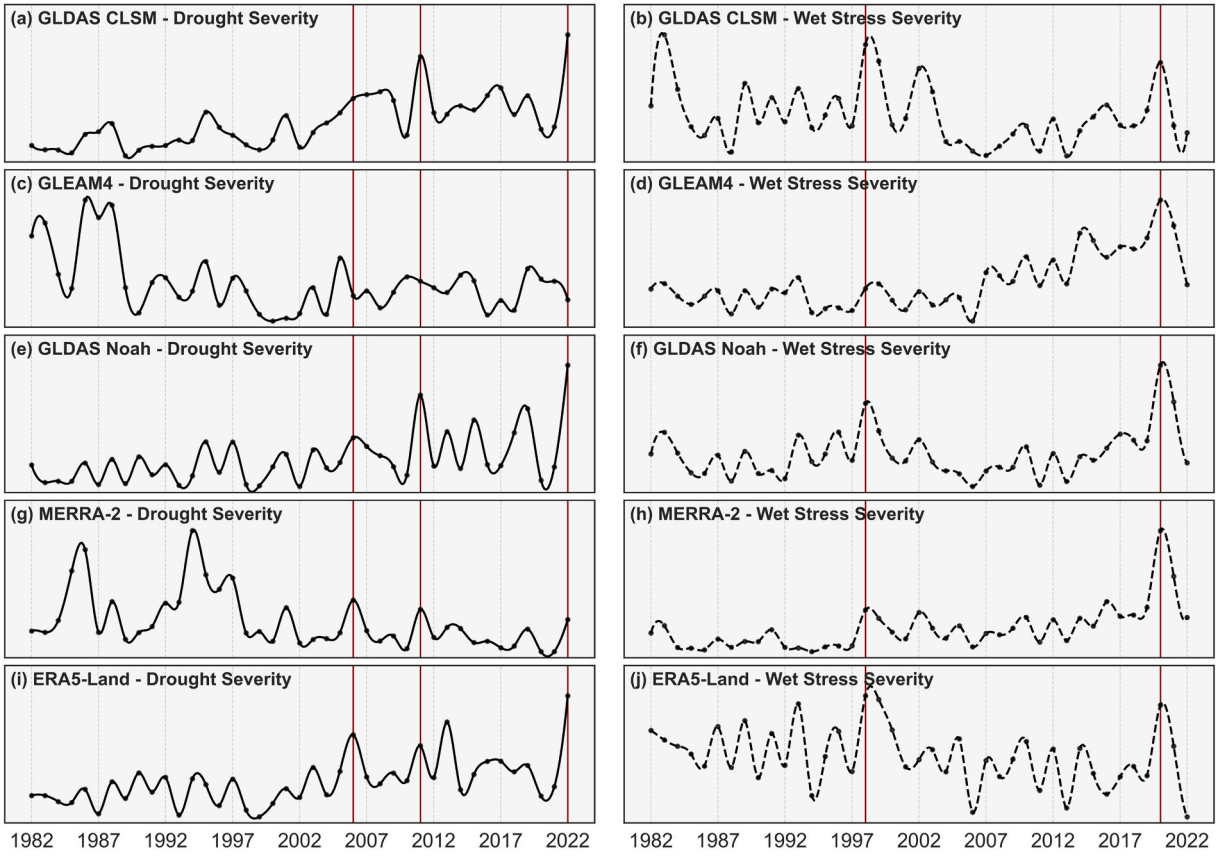

Fig. 9. Time series of summer (June–August) drought intensity and wet stress intensity over the Yangtze River Basin for each product. Red vertical lines indicate years of documented extreme events. The y-axes represent annual drought severity (a, c, e, g, i) and wet stress severity (b, d, f, h, j), respectively.

this agreement does not imply consistent hydrological behavior. For example, ERA5-Land and GLDAS_CLSM both indicate drying in Northeast China, yet differ substantially in their correlation with short-term observations and event-phase responses. These discrepancies stem not only from temporal smoothing or spatial resolution but also from differences in soil depth sensitivity, energy balance closure, and memory representation. Such divergences are especially pronounced in transitional regions like the Loess Plateau, where rainfall infiltration and land–atmosphere feedbacks vary significantly. Prior studies have emphasized the role of SM persistence in modulating climate interactions (Seneviratne et al., 2010), and our findings highlight the need to consider memory characteristics when assessing product consistency across timescales. In irrigated regions such as the Huang–Huai–Hai Plain, ERA5-Land exhibits a pronounced drying signal that contrasts with documented agricultural intensification and irrigation expansion (Liu et al., 2025; Piao et al., 2010). This highlights that product-derived

trends may partly reflect model structural limitations in representing human–water interactions, rather than purely climate-driven changes.

Among the evaluated products, ERA5-Land shows the highest NDWI agreement with manual in situ observations, reflecting its stability in trend detection. However, despite its spatially consistent performance, its regional correlation with SMAP L4 remains relatively low. In contrast, MERRA-2 shows the strongest agreement with SMAP L4 in both SM and NDWI, indicating higher sensitivity to regional anomalies and hydrological variability. This discrepancy raises a relevant consideration: SMAP L4 may face certain limitations when applied to dry–wet intensity trend detection over extended time series.

To better capture trend sensitivity and directional asymmetry, the Net Dry–Wet Intensity (NDWI) was introduced, which integrates positive and negative anomalies into a unified signal. Unlike traditional drought indices that focus solely on deficit conditions, NDWI explicitly frames soil water stress in a bidirectional sense, thereby addressing both drought and wet stress anomalies relevant for agricultural systems. This concept, rooted in SM memory theory (Seneviratne et al., 2006), aligns with observed patterns: ERA5-Land exhibits the highest NDWI coherence with manual in situ data, while GLEAM and MERRA-2 capture more pronounced short-term NDWI fluctuations during hydrological extremes but show weaker alignment with long-term directional shifts. While NDWI was designed to capture memory effects by integrating directional anomalies, its formulation is theoretically supported by soil moisture persistence theory, which emphasizes that anomalies in one direction (e.g., deficit) alter subsequent land–atmosphere fluxes differently than anomalies in the opposite direction (e.g., excess). By combining positive and negative deviations into a unified trajectory, NDWI inherently encodes such asymmetric memory, reducing signal cancellation that is common in percentile-based indices. Although explicit validation of its "memory encoding" (e.g., via lag correlation or comparison with established drought indices) was not undertaken here, the theoretical foundation lends confidence in its capacity to represent soil moisture memory. Further empirical testing remains an important next step. These results support NDWI as a robust tool for harmonizing SM trend assessment across diverse observational and reanalysis datasets.

4.3. Toward climate-aware fusion solutions

Spatial inconsistencies among SM products—particularly in transition zones like the Loess Plateau and North China Plain—underscore the need for climate-aware fusion strategies tailored to agricultural water management, where reliable soil moisture information is critical for crop growth monitoring, irrigation scheduling, and drought early warning. These regions are hydrologically complex and agriculturally critical, with variable rainfall, high irrigation demand, and strong land–atmosphere feedbacks. Divergence among products in such zones compromises the reliability of SM-based assessments when applied in practice. For instance, models like GLDAS_CLSM underperform due to shallow soil depths (~2 cm) and parameter sensitivity, while ERA5-Land, though more stable, lacks sub-kilometer resolution needed to capture field-scale heterogeneity.

We propose that SM fusion systems designed for agricultural applications should incorporate: (1) Vertical coherence, to integrate surface and root-zone information and thereby reduce depth-related uncertainty; (2) Memory-informed weighting, to balance long-term stability (e.g., ERA5-Land) with short-term anomaly sensitivity (e.g., MERRA-2); (3) Region-specific calibration, to explicitly account for irrigation effects and crop-specific water requirements in human-managed landscapes; (4) Uncertainty-aware ensembles, to formally propagate product divergence into drought and wet stress indices and provide confidence bounds for decision-making. Machine learning–based downscaling offers potential to address spatial mismatches (e.g., SMAP vs. coarse products), but requires denser in situ networks than are currently available (Karthikeyan and Mishra, 2021). In the meantime, ensemble fusion—combining ERA5-Land's trend fidelity, GLEAM4's anomaly detection, and MERRA-2's radiance sensitivity—can enhance robustness. The use of physically meaningful indices such as NDWI further strengthens comparability and interpretability across products. Such fusion frameworks would not only improve technical consistency but also provide more actionable support for agricultural water management under a changing climate.

5. Conclusion

This study provides a comprehensive benchmark evaluation of five widely used long time-series SM products—ERA5-Land, GLEAM4, GLDAS_Noah, GLDAS_CLSM, and MERRA-2—across China over the period 1982–2022. By integrating in situ observations, SMAP-L4 satellite data, and records of major drought and flood events, we systematically assessed product reliability, spatial consistency, and their ability to capture hydroclimatic extremes relevant for agricultural water stress monitoring.

Our results highlight clear divergences: MERRA-2, GLEAM4, and GLDAS_Noah indicate widespread wetting, while ERA5-Land and GLDAS_CLSM depict drying signals. Among the products, ERA5-Land demonstrates the most reliable long-term trend detection and consistent agreement with manual in situ observations, making it the preferred benchmark for multi-decadal monitoring. In contrast, MERRA-2 shows the strongest agreement with SMAP-L4, reflecting its strength in short-term anomaly detection despite systematic wetting biases. These complementary characteristics underscore that no single product can fully capture the complexity of SM variability across transitional and irrigated regions such as the Loess Plateau and Huang–Huai–Hai Plain.

Importantly, this evaluation reveals dataset-specific advantages and constraints that should be carefully considered in agricultural applications. While the study provides a robust framework for benchmarking, several limitations remain. Specifically, our analysis focused on surface (0–10 cm) SM rather than the root zone, did not explicitly incorporate irrigation practices or crop-specific thresholds, and relied on a relatively short validation period with SMAP compared to the multi-decadal record. These factors may influence the direct transferability of findings to operational agricultural water management.

Despite these limitations, the study delivers three key contributions: (1) it establishes a systematic benchmark of consistency and divergences across widely used SM datasets, (2) it introduces the Net Dry–Wet Intensity (NDWI) as a complementary metric for capturing asymmetric drought and wet stress signals, and (3) it identifies priority regions and processes where product improvement and fusion are most needed. Taken together, these findings provide an essential foundation for advancing SM applications in agricultural water stress monitoring, and point toward future improvements through root-zone integration, irrigation-aware modeling, and uncertainty-aware ensembles tailored to agro-climatic contexts.

CRediT authorship contribution statement

Qiang Yu: Writing – review & editing, Funding acquisition. **Ermao Ding:** Writing – review & editing, Formal analysis. **Xuetong Wang:** Writing – review & editing, Data curation. **Liang He:** Funding acquisition, Conceptualization. **Peng Li:** Writing – original draft, Validation, Software, Methodology.

Declaration of Competing Interest

The authors declare that they have no known competing financial interests or personal relationships that could have appeared to influence the work reported in this paper.

Acknowledgements

This work was supported by the National Natural Science Foundation of China (No. 42375195).

Data availability

Data will be made available on request.

References

Albergel, C., De Rosnay, P., Gruhier, C., Muñoz-Sabater, J., Hasenauer, S., Isaksen, L., Kerr, Y., Wagner, W., 2012. Evaluation of remotely sensed and modelled soil moisture products using global ground-based in situ observations. Remote Sens. Environ. 118, 215–226. https://doi.org/10.1016/j.rse.2011.11.017.

Albergel, C., Dorigo, W., Reichle, R.H., Balsamo, G., Rosnay, P. de, Muñoz-Sabater, J., Isaksen, L., Jeu, R. de, Wagner, W., 2013. Skill and Global Trend Analysis of Soil Moisture from Reanalyses and Microwave Remote Sensing. https://doi.org/10.1175/JHM-D-12-0161.1.

Carrão, H., Russo, S., Sepulcre-Canto, G., Barbosa, P., 2016. An empirical standardized soil moisture index for agricultural drought assessment from remotely sensed data. Int. J. Appl. Earth Obs. Geoinf. 48, 74–84. https://doi.org/10.1016/j.jag.2015.06.011.

Chan, S.K., Bindlish, R., O'Neill, P., Jackson, T., Njoku, E., Dunbar, S., Chaubell, J., Piepmeier, J., Yueh, S., Entekhabi, D., Colliander, A., Chen, F., Cosh, M.H., Caldwell, T., Walker, J., Berg, A., McNairn, H., Thibeault, M., Martínez-Fernández, J., Uldall, F., Seyfried, M., Bosch, D., Starks, P., Holifield Collins, C., Prueger, J., van der Velde, R., Asanuma, J., Palecki, M., Small, E.E., Zreda, M., Calvet, J., Crow, W.T., Kerr, Y., 2018. Development and assessment of the SMAP enhanced passive soil moisture product. Remote Sens. Environ. 204, 931–941. https://doi.org/10.1016/j.rse.2017.08.025.

Chen, L., Brun, P., Buri, P., Fatichi, S., Gessler, A., McCarthy, M.J., Pellicciotti, F., Stocker, B., Karger, D.N., 2025. Global increase in the occurrence and impact of multiyear droughts. Science. https://doi.org/10.1126/science.ado4245.

Dorigo, W., de Jeu, R., Chung, D., Parinussa, R., Liu, Y., Wagner, W., Fernández-Prieto, D., 2012. Evaluating global trends (1988–2010) in harmonized multi-satellite surface soil moisture. Geophys. Res. Lett. 39. https://doi.org/10.1029/2012GL052988.

Dorigo, W., Wagner, W., Albergel, C., Albrecht, F., Balsamo, G., Brocca, L., Chung, D., Ertl, M., Forkel, M., Gruber, A., Haas, E., Hamer, P.D., Hirschi, M., Ikonen, J., De Jeu, R., Kidd, R., Lahoz, W., Liu, Y.Y., Miralles, D., Mistelbauer, T., Nicolai-Shaw, N., Parinussa, R., Pratola, C., Reimer, C., Van Der Schalie, R., Seneviratne, S.I., Smolander, T., Lecomte, P., 2017. ESA CCI soil moisture for improved earth system understanding: State-of-the art and future directions. Remote Sens. Environ. 203, 185–215. https://doi.org/10.1016/j.rse.2017.07.001.

Dorigo, W.A., Gruber, A., De Jeu, R.A.M., Wagner, W., Stacke, T., Loew, A., Albergel, C., Brocca, L., Chung, D., Parinussa, R.M., Kidd, R., 2015. Evaluation of the ESA CCI soil moisture product using ground-based observations. Remote Sens. Environ. 162, 380–395. https://doi.org/10.1016/j.rse.2014.07.023.

Edwards, B., Gray, M., Hunter, B., 2019. The social and economic impacts of drought. Aust. J. Soc. Issues 54, 22–31. https://doi.org/10.1002/ajs4.52.

Gavrilov, M.B., Marković, S.B., Janc, N., Nikolić, M., Valjarević, A., Komac, B., Zorn, M., Punišić, M., Bačević, N., 2018. Assessing average annual air temperature trends using the Mann–Kendall test in Kosovo. Acta Geogr. Slov. 58, 7–25. https://doi.org/10.3986/AGS.1309.

Gelaro, R., McCarty, W., Suárez, M.J., Todling, R., Molod, A., Takacs, L., Randles, C.A., Darmenov, A., Bosilovich, M.G., Reichle, R., Wargan, K., Coy, L., Cullather, R., Draper, C., Akella, S., Buchard, V., Conaty, A., Silva, A.M. da, Gu, W., Kim, G.-K., Koster, R., Lucchesi, R., Merkova, D., Nielsen, J.E., Partyka, G., Pawson, S., Putman, W., Rienecker, M., Schubert, S.D., Sienkiewicz, M., Zhao, B., 2017. The Modern-Era Retrospective Analysis for Research and Applications, Version 2 (MERRA-2). https://doi.org/10.1175/JCLI-D-16-0758.1.

Guan, Y., Gu, X., Slater, L.J., Li, J., Kong, D., Zhang, X., 2023. Spatio-temporal variations in global surface soil moisture based on multiple datasets: intercomparison and climate drivers. J. Hydrol. 625, 130095. https://doi.org/10.1016/j.jhydrol.2023.130095.

Guo, X., Zhu, A.L., Chen, R., Li, Q., Li, Y., Luo, Y., Yin, C., Cai, Y., Xia, Z., 2025. Flood disaster management neglects rural areas. Nat. Food 1–2. https://doi.org/10.1038/s43016-025-01171-6.

Han, J., Fang, S., Wang, X., Zhuo, W., Yu, Y., Peng, X., Zhang, Y., 2024. The impact of intra-annual temperature fluctuations on agricultural temperature extreme events and attribution analysis in mainland China. Sci. Total Environ. 949, 174904. https://doi.org/10.1016/j.scitotenv.2024.174904.

Hersbach, H., Bell, B., Berrisford, P., Hirahara, S., Horányi, A., Muñoz-Sabater, J., Nicolas, J., Peubey, C., Radu, R., Schepers, D., Simmons, A., Soci, C., Abdalla, S., Abellan, X., Balsamo, G., Bechtold, P., Biavati, G., Bidlot, J., Bonavita, M., Chiara, G. D., Dahlgren, P., Dee, D., Diamantakis, M., Dragani, R., Flemming, J., Forbes, R., Fuentes, M., Geer, A., Haimberger, L., Healy, S., Hogan, R.J., Hólm, E., Janisková, M., Keeley, S., Laloyaux, P., Lopez, P., Lupu, C., Radnoti, G., Rosnay, P. de, Rozum, I., Vamborg, F., Villaume, S., Thépaut, J.-N., 2020. The ERA5 global reanalysis. Q. J. R. Meteorol. Soc. 146, 1999–2049. https://doi.org/10.1002/qj.3803.

Hirschi, M., Stradiotti, P., Crezee, B., Dorigo, W., Seneviratne, S.I., 2025. Potential of long-term satellite observations and reanalysis products for characterising soil drying: trends and drought events. Hydrol. Earth Syst. Sci. 29, 397–425. https://doi.org/10.5194/hess-29-397-2025.

Hong, X., Jia, S., Zhu, W., Song, Z., 2024. Evaluation of global seamless soil moisture products over China: a perspective of soil moisture sensitivity to precipitation. J. Hydrol. 641, 131789. https://doi.org/10.1016/j.jhydrol.2024.131789.

Hou, Y., Zhang, M., Wei, X., Liu, S., Li, Q., Cai, T., Liu, W., Zhao, R., Liu, X., 2021. Quantification of ecohydrological sensitivities and their influencing factors at the seasonal scale. Hydrol. Earth Syst. Sci. 25, 1447–1466. https://doi.org/10.5194/hess-25-1447-2021.

Hu, X., Hall, J.W., Shi, P., Lim, W.H., 2016. The spatial exposure of the Chinese infrastructure system to flooding and drought hazards. Nat. Hazards 80, 1083–1118. https://doi.org/10.1007/s11069-015-2012-3.

Ji, J., Sun, M., Ji, G., Li, L., Chen, W., Huang, J., Guo, Y., 2025. Simulation of actual evaporation and its multi-time scale attribution analysis for major rivers in China. J. Hydrol. 657, 133121. https://doi.org/10.1016/j.jhydrol.2025.133121.

Jose, V., Chandrasekar, A., Reddy Rodda, S., 2024. Impact of historical land cover changes on land surface characteristics over the Indian region using land information system. Pure Appl. Geophys 181, 2561–2588. https://doi.org/10.1007/s00024-024-03523-y.

Karthikeyan, L., Mishra, A.K., 2021. Multi-layer high-resolution soil moisture estimation using machine learning over the United States. Remote Sens. Environ. 266, 112706. https://doi.org/10.1016/j.rse.2021.112706.

Kaur, G., Zurweller, B.A., Nelson, K.A., Motavalli, P.P., Dudenhoeffer, C.J., 2017. Soil waterlogging and nitrogen fertilizer management effects on corn and soybean yields. Agron. J. 109, 97–106. https://doi.org/10.2134/agronj2016.07.0411.

Khan, I., Islam, Md.R., 2025. Earth observation Data-Based assessment of the impacts of June 2024 flooding in sylhet division of Bangladesh. S2666592125000095 Nat. Hazards Res.. https://doi.org/10.1016/j.nhres.2025.01.009.

Konkathi, P., Karthikeyan, L., 2024. Utility of L-band and X-band vegetation optical depth to examine vegetation response to soil moisture droughts in south Asia. Remote Sens. Environ. 301, 113933. https://doi.org/10.1016/j.rse.2023.113933.

Li, Q., Shi, G., Shangguan, W., Nourani, V., Li, J., Li, L., Huang, F., Zhang, Y., Wang, C., Wang, D., Qiu, J., Lu, X., Dai, Y., 2022. A 1 km daily soil moisture dataset over China using in situ measurement and machine learning. Earth Syst. Sci. Data 14, 5267–5286. https://doi.org/10.5194/essd-14-5267-2022.

Ling, X., Huang, Y., Guo, W., Wang, Y., Chen, C., Qiu, B., Ge, J., Qin, K., Xue, Y., Peng, J., 2021. Comprehensive evaluation of satellite-based and reanalysis soil moisture products using in situ observations over China. Hydrol. Earth Syst. Sci. 25, 4209–4229. https://doi.org/10.5194/hess-25-4209-2021.

Liu, G., Wang, W., Xu, H., 2025. Irrigation-induced decreases in reference evapotranspiration over the north China plain. Atmos. Res 314, 107798. https://doi.org/10.1016/j.atmosres.2024.107798.

Liu, Yongwei, Liu, Yuanbo, Wang, W., 2019. Inter-comparison of satellite-retrieved and global land data assimilation System-simulated soil moisture datasets for global drought analysis. Remote Sens. Environ. 220, 1–18. https://doi.org/10.1016/j.rse.2018.10.026.

Lucas, R., Van De Kerchove, R., Otero, V., Lagomasino, D., Fatoyinbo, L., Omar, H., Satyanarayana, B., Dahdouh-Guebas, F., 2020. Structural characterisation of mangrove forests achieved through combining multiple sources of remote sensing data. Remote Sens. Environ. 237, 111543. https://doi.org/10.1016/j.rse.2019.111543.

Luo, M., Sa, C., Meng, F., Duan, Y., Liu, T., Bao, Y., 2021. Assessing remotely sensed and reanalysis products in characterizing surface soil moisture in the Mongolian plateau. Int. J. Digit. Earth.

Martens, B., Miralles, D.G., Lievens, H., van der Schalie, R., de Jeu, R.A.M., Fernández-Prieto, D., Beck, H.E., Dorigo, W.A., Verhoest, N.E.C., 2017. GLEAM v3: satellite-based land evaporation and root-zone soil moisture. Geosci. Model Dev. 10, 1903–1925. https://doi.org/10.5194/gmd-10-1903-2017.

Miralles, D.G., Bonte, O., Koppa, A., Baez-Villanueva, O.M., Tronquo, E., Zhong, F., Beck, H.E., Hulsman, P., Dorigo, W., Verhoest, N.E.C., Haghdoost, S., 2025. GLEAM4: global land evaporation and soil moisture dataset at 0.1° resolution from 1980 to near present. Sci. Data 12, 416. https://doi.org/10.1038/s41597-025-04610-y.

Muñoz-Sabater, J., Dutra, E., Agustí-Panareda, A., Albergel, C., Arduini, G., Balsamo, G., Boussetta, S., Choulga, M., Harrigan, S., Hersbach, H., Martens, B., Miralles, D.G., Piles, M., Rodríguez-Fernández, N.J., Zsoter, E., Buontempo, C., Thépaut, J.-N., 2021a. ERA5-Land: a state-of-the-art global reanalysis dataset for land applications. Earth Syst. Sci. Data 13, 4349–4383. https://doi.org/10.5194/essd-13-4349-2021.

Niu, X., Tang, J., Chen, D., Wang, S., Ou, T., 2021. Elevation-Dependent warming over the Tibetan plateau from an ensemble of CORDEX-EA regional climate simulations. J. Geophys. Res. Atmospheres 126, e2020JD033997. https://doi.org/10.1029/2020JD033997.

Piao, S., Ciais, P., Huang, Y., Shen, Z., Peng, S., Li, J., Zhou, L., Liu, H., Ma, Y., Ding, Y., Friedlingstein, P., Liu, C., Tan, K., Yu, Y., Zhang, T., Fang, J., 2010. The impacts of climate change on water resources and agriculture in China. Nature 467, 43–51. https://doi.org/10.1038/nature09364.

Qiu, J., Gao, Q., Wang, S., Su, Z., 2016. Comparison of temporal trends from multiple soil moisture data sets and precipitation: the implication of irrigation on regional soil moisture trend. Int. J. Appl. Earth Obs. Geoinf. Adv. Valid. Appl. Remote. Sense Soil Moisture Part 2 48, 17–27. https://doi.org/10.1016/j.jag.2015.11.012.

Rahmani, A., Golian, S., Brocca, L., 2016. Multiyear monitoring of soil moisture over Iran through satellite and reanalysis soil moisture products. Int. J. Appl. Earth Obs. Geoinf. Adv. Valid. Appl. Remote. Sense Soil Moisture Part 2 48, 85–95. https://doi.org/10.1016/j.jag.2015.06.009.

Řehoř, J., Trnka, M., Brázdil, R., Fischer, M., Balek, J., van der Schrier, G., Feng, S., 2023. Global hotspots in soil moisture-based drought trends. Environ. Res. Lett. 19, 014021. https://doi.org/10.1088/1748-9326/ad0f01.

Reichle, R.H., Draper, C.S., Liu, Q., Girotto, M., Mahanama, S.P.P., Koster, R.D., Lannoy, G.J.M.D., 2017. Assessment of MERRA-2 Land Surface Hydrology Estimates. https://doi.org/10.1175/JCLI-D-16-0720.1.

Rodell, M., Houser, P.R., Jambor, U., Gottschalck, J., Mitchell, K., Meng, C.-J., Arsenault, K., Cosgrove, B., Radakovich, J., Bosilovich, M., Entin, J.K., Walker, J.P., Lohmann, D., Toll, D., 2004. The Global Land Data Assimilation System. https://doi.org/10.1175/BAMS-85-3-381.

Schober, P., Boer, C., Schwarte, L.A., 2018. Correlation coefficients: appropriate use and interpretation. Anesth. Analg. 126, 1763. https://doi.org/10.1213/ANE.0000000000002864.

Schroeter, S.A., Orme, A.M., Lehmann, K., Lehmann, R., Chaudhari, N.M., Küsel, K., Wang, H., Hildebrandt, A., Totsche, K.U., Trumbore, S., Gleixner, G., 2025. Hydroclimatic extremes threaten groundwater quality and stability. Nat. Commun. 16, 720. https://doi.org/10.1038/s41467-025-55890-2.

Sedgwick, P., 2014. Spearman's rank correlation coefficient. BMJ 349, g7327. https://doi.org/10.1136/bmj.g7327.

Seneviratne, S.I., Koster, R.D., Guo, Z., Dirmeyer, P.A., Kowalczyk, E., Lawrence, D., Liu, P., Mocko, D., Lu, C.-H., Oleson, K.W., Verseghy, D., 2006. Soil Moisture Memory in AGCM Simulations: Analysis of Global Land–Atmosphere Coupling Experiment (GLACE) Data. https://doi.org/10.1175/JHM533.1.

Seneviratne, S.I., Corti, T., Davin, E.L., Hirschi, M., Jaeger, E.B., Lehner, I., Orlowsky, B., Teuling, A.J., 2010. Investigating soil moisture–climate interactions in a changing climate: a review. Earth-Sci. Rev. 99, 125–161. https://doi.org/10.1016/j.earscirev.2010.02.004.

Shu, P., Zhou, W., Putnam, A.E., Li, B., Kang, S., Sha, Y., Shi, Z., Ming, G., Wang, H., Sun, Y., Wright, D.K., Liu, W., Liu, X., Cheng, P., Song, Y., Niu, D., Dodson, J.R., Du, H., Zhao, J., Zhang, Z., Qiu, Y., An, Z., 2025. Intensified monsoonal rainstorm events over westerly-dominated asian interior during the warm mid-Holocene. Commun. Earth Environ. 6, 1–12. https://doi.org/10.1038/s43247-025-02005-w.

Vannest, K.J., Parker, R.I., Davis, J.L., Soares, D.A., Smith, S.L., 2012. The Theil–Sen slope for High-Stakes decisions from progress monitoring. Behav. Disord. 37, 271–280. https://doi.org/10.1177/019874291203700406.

Wang, A., Shi, X., 2019. A Multilayer Soil Moisture Dataset Based on the Gravimetric Method in China and Its Characteristics. https://doi.org/10.1175/JHM-D-19-0035.1.

Wang, H., 2025. Has global warming already increased precipitation variability and disaster risk in past century? Sci. China Earth Sci. 68, 646–648. https://doi.org/10.1007/s11430-024-1494-8.

Wang, J., Liu, W., Yin, D., 2025. Impacts of integrated meteorological and agricultural drought on global maize yields. Agric. Water Manag. 318, 109727. https://doi.org/10.1016/j.agwat.2025.109727.

Wang, S., Ancell, B., Yang, Z.-L., Duan, Q., Anagnostou, E.N., 2022. Hydroclimatic extremes and impacts in a changing environment: observations, mechanisms, and projections. J. Hydrol. 608, 127615. https://doi.org/10.1016/j.jhydrol.2022.127615.

Wang, X., Yu, Q., 2005. Unbiasedness of the Theil–Sen estimator. J. Nonparametr. Stat. 17, 685–695. https://doi.org/10.1080/10485250500039452.

Xu, X., Wang, X., Xiao, J., Zhang, S., Yang, Y., Li, X., Sha, T., Li, Z., 2025. Inconsistencies in global soil moisture products and discrepancies in their relationship with vegetation productivity. J. Hydrol. 659, 133298. https://doi.org/10.1016/j.jhydrol.2025.133298.

Yue, S., Wang, C.Y., 2002. Applicability of prewhitening to eliminate the influence of serial correlation on the Mann-Kendall test. Water Resour. Res. 38, 4-1–4–7. https://doi.org/10.1029/2001WR000861.

Zeng, J., Li, Z., Chen, Q., Bi, H., Qiu, J., Zou, P., 2015. Evaluation of remotely sensed and reanalysis soil moisture products over the Tibetan plateau using in-situ observations. Remote Sens. Environ. 163, 91–110. https://doi.org/10.1016/j.rse.2015.03.008.

Zeng, X., Decker, M., 2009. Improving the Numerical Solution of Soil Moisture–Based Richards Equation for Land Models with a Deep or Shallow Water Table. https://doi.org/10.1175/2008JHM1011.1.

Zhang, X., Yuan, X., Liu, H., Gao, H., Wang, X., 2022. Soil moisture estimation for Winter-Wheat waterlogging monitoring by assimilating remote sensing inversion data into the distributed hydrology soil vegetation model. Remote Sens. 14, 792. https://doi.org/10.3390/rs14030792.